Commun Nonlinear Sci Numer Simulat 16 (2011) 2894–2906

Contents lists available at ScienceDirect

Commun Nonlinear Sci Numer Simulat

journal homepage: www.elsevier.com/locate/cnsns

The rank of a sequence as an indicator of chaos in discrete nonlinear dynamical systems

Minvydas Ragulskis [a,*], Zenonas Navickas [b,1]

[a] Research Group for Mathematical and Numerical Analysis of Dynamical Systems, Kaunas University of Technology, Studentu 50-222, Kaunas LT-51368, Lithuania
[b] Department of Applied Mathematics, Kaunas University of Technology, Studentu 50-325, Kaunas LT-51368, Lithuania

ARTICLE INFO

Article history:
Received 27 April 2010
Received in revised form 22 September 2010
Accepted 5 October 2010
Available online 28 October 2010

Keywords:
Hankel matrix
Rank of a sequence
Iterative map
Chaos

ABSTRACT

An alternative technique for clocking the convergence of iterative chaotic maps is proposed in this paper. It is based on the concept of the Hankel rank of a solution of the discrete nonlinear dynamical system. Computation and visualization of pseudoranks in the space of system's parameters and initial conditions provides the insight into the fractal nature of the dynamical attractor and reveals the stable, the unstable manifold and the convergence properties of the system. All these manifolds are produced by a simple and a straightforward computational rule and are intertwined in one figure. On the other hand, the computation of ranks of subsequences of solutions helps to identify and assess the sensitivity of the system to initial conditions and can be used as a simple and effective numerical tool for qualitative investigation of discrete iterative maps.

1. Introduction

Clocking convergence is an important tool for investigating various aspects of iterative maps, especially chaotic maps. The rate of convergence to the critical attractor when an ensemble of initial conditions is uniformly spread over the entire phase space may provide the insight into the fractal nature and the scale invariance of the dynamical attractor [1,2]. Though the detailed structure of patterns of the stable and the unstable manifolds of the period-doubling cascade of the logistic map is presented in [3], the speed of convergence to the fractal structure of the intertwined manifolds is still an interesting topic of research. Numerical convergence of the discrete logistic map gauged with a finite computational accuracy is investigated in [4]. The numerical study in [4] reveals that the numerical convergence maps of the logistic map form interesting self-similar patterns before the onset to chaos. Questions centered on how numerical convergent behaviors change as the system evolves to chaos are left out of scope in [4]. The main objective of this paper is to address these questions, but using different computational instruments. We introduce the concept of the rank of a sequence based on the Hankel matrix.

The Hankel matrix, named after Hermann Hankel, is widely used for system identification when given a sequence of output data and a realization of an underlying state-space model is desired. A first solution to this challenging system-theoretic problem that became known as the statespace realization problem was provided in 1965 in [5]. The key tool for solving this problem is the Hankel matrix, whose factorization into the product of an observability matrix and controllability matrix is known as the Ho-Kalman realization method [5]. The Hankel matrix-based models are appropriate to describe linear input/output mappings by infinitely many parameters, in general, since they might be obtained directly from available input/out-

* Corresponding author. Tel.: +370 69822456; fax: +370 37330446.
E-mail addresses: minvydas.ragulskis@ktu.lt (M. Ragulskis), zenonas.navickas@ktu.lt (Z. Navickas).
URL: http://www.personalas.ktu.lt/~mragul (M. Ragulskis).
[1] Tel.: +370 68223789.

1007-5704/$ - see front matter © 2010 Elsevier B.V. All rights reserved.
doi:10.1016/j.cnsns.2010.10.008

put data on the system. It took years of research to go from the theoretical results described in [5] to a numerically reliable realization algorithm [6].

The combination of deterministic realization theory based on the factorization of the Hankel matrix, with the theory of Markovian and innovations representations, gave rise to the stochastic theory of minimal realizations. The stochastic realization problem was studied intensively during the early 1970s in connection with innovations theory and spectral factorization theory [7,8].

Many new innovative applications based on the Hankel matrix have been developed in diverse areas of science and engineering. Gathering outputs from an impulse-response simulation into a generalized Hankel matrix and its singular value decomposition (SVD) helps to obtain reduced order models for high dimensional linear dynamical systems [9]. An infinite polynomial block Hankel matrix, as well as its associate τ-finite polynomial block Hankel matrices, is used in [10–14] in order to relate the spectral controllability and observability properties of minimal realizations with the minimum feasible finite rank of such a Hankel matrix. Realization and partial realization theories for linear time invariant systems being subject to a set of incommensurate internal and external point delays are investigated in [15] using truncated and infinite block Hankel matrixes.

Hankel matrix is used to expand the original time series into the trajectory matrix of the system in [16]; singular value decomposition of the trajectory matrix helps to forecast paroxysmal events. Hankel transform of an integer sequence is defined in [17] and used to classify certain integer sequences. Hankel rank is defined in [18] and used to express solutions of nonlinear differential equations in forms comprising ratios of finite sums of standard functions [19–21].

We will exploit the Hankel rank for the quantitative description of solutions of discrete nonlinear dynamical systems in this paper. This paper is organized as follows. The rank of a sequence is defined in Section 2; ranks for orbits generated by the logistic map are computed in Section 3; backward iterations of the logistic map are discussed in Section 4; the concept of the new indicator of chaos is introduced in Section 5; computational experiments with the Henon map are done in Section 6; concluding remarks are given in Section 7.

2. The definition of the rank of a sequence

Let S is a sequence of real or complex numbers:

$$S := (x_0, x_1, x_2, \ldots) := (x_k; k \in Z_0) \tag{1}$$

A subsequence of S is denoted by S_j; $j = 0,1,2,\ldots$:

$$(x_j, x_{j+1}, x_{j+2}, \ldots) := S_j \tag{2}$$

It can be noted that $S = S_0$. The Hankel matrix H can be constructed from the sequence S:

$$H := \begin{bmatrix} x_0 & x_1 & x_2 & \cdots \\ x_1 & x_2 & x_3 & \cdots \\ \cdots & \cdots & \cdots & \cdots \end{bmatrix} \tag{3}$$

Minors $H_j^{(m)}$ of H are defined as follows:

$$H_j^{(m)} := [x_{r+s-2+j}]_{1\leqslant r,s\leqslant m} = \begin{bmatrix} x_j & x_{j+1} & \cdots & x_{j+m-1} \\ x_{j+1} & x_{j+2} & \cdots & x_{j+m} \\ & & \cdots & \\ x_{j+m-1} & x_{j+m} & \cdots & x_{j+2m-2} \end{bmatrix} \tag{4}$$

Determinants of these minors are denoted by $d_j^{(m)} : \det H_j^{(m)} = d_j^{(m)}$.

Definition 1. The rank of a subsequence S_j is such natural number m_j that satisfies the following condition (if the rank exists):

$$d_j^{(m_j+k)} = 0 \tag{5}$$

for all $k \in N$; when $d_j^{(m_j)} \neq 0$.

We will use the following notation:

$$m_j = Hr(x_j, x_{j+1}, \ldots) = HrS_j \tag{6}$$

If such number m_j does not exist, we will note that the subsequence S_j does not have a rank: $HrS_j := +\infty$.

Corollary 1. *If $HrS_{j_0} = m_{j_0} < +\infty$ holds true for any j_0, then finite m_j exist for all $j = 0,1,2,\ldots$. Moreover,*

$$m_0 \geqslant m_1 \geqslant m_2 \geqslant \cdots, \tag{7}$$

when $|m_j - m_{j+1}| \leqslant 1$.

Corollary 2. *If $m_{j_0} = +\infty$ holds true for any j_0, then*

$$m_j = +\infty \tag{8}$$

for all $j = 0,1,2,\ldots$.

Definition 2. The rank of a sequence S is a number m_0 if only $m_0 < +\infty$:

$$HrS = m_0 \tag{9}$$

Otherwise, the sequence S does not have a rank:

$$HrS = +\infty \tag{10}$$

Comment 1. By definition we will assume that

$$Hr(0,0,0,\ldots) := 0 \tag{11}$$

Example 1. Let $S := (1,1,1,0,0,\ldots)$. Then, $HrS = HrS_0 = 3$; $HrS_1 = 2$; $HrS_2 = 1$; $HrS_j = 0$ for $j = 3,4,\ldots$.

Example 2. Let $S := (j; j \in Z_0)$. Then, $d_j^{(1)} = |j| = j$; $d_j^{(2)} = \begin{vmatrix} j & j+1 \\ j+1 & j+2 \end{vmatrix} = -1$; but $d_j^{(m)} = 0$ for $m = 3,4,\ldots$ for all $j \in Z_0$. Therefore $HrS = HrS_j = 2$ for all $j \in Z_0$.

Example 3. Let $S := (j!; j \in Z_0)$. Then, $HrS = HrS_j = +\infty$ for all $j \in Z_0$. Thus, the given sequence of factorials does not have a rank.

Definition 3. Let the sequence $S = (x_0, x_1, x_2, \ldots)$ and arbitrary numbers $x_{-k}, x_{-k+1}, \ldots, x_{-1}$ are given. Then the sequence $S_{-k} := (x_{-k}, x_{-k+1}, \ldots, x_{-1}, x_0, x_1, x_2, \ldots)$ is the expansion of the sequence S.

Corollary 3. *The following estimation holds true:*

$$HrS_{-k} \leqslant k + HrS \tag{12}$$

Example 4. Let $S := (1,0,0,\ldots)$; then $HrS = 1$. The following equality holds for arbitrary $x_{-k}, x_{-k+1}, \ldots, x_{-1} \in R$: $Hr(x_{-k}, x_{-k+1}, \ldots, x_{-1}, 1, 0, 0, \ldots) = k + 1$.

Example 5. Let $S := (0,1,2,3,\ldots)$; then $HrS = 2$. Then, $Hr(-k, -k+1, \ldots, -1, 0, 1, 2, 3, \ldots) = 2$ for all $k \in N$.

Example 6. Let $S_{-k} := (x_{-k}, x_{-k+1}, x_{-k+2}, \ldots, x_{-2}, x_{-1}, (1 - \frac{1}{A}), (1 - \frac{1}{A}), \ldots)$; $x_{-k}, x_{-k+1}, \ldots, x_{-2}, x_{-1} \in R$; $A \neq 0$. Then $HrS_{-k} \leqslant k + 1$; $HrS_{-k+1} \leqslant k$; $HrS_{-k+2} \leqslant k - 1; \ldots$; $HrS_{-1} \leqslant 2$; $HrS_j = 1$ for all $j = 0,1,2,\ldots$ and $A \neq 1$. It can be noted that $HrS_j = 0$ for all $j = 0,1,2,\ldots$ and $A = 1$. The lower or equal sign in the previous inequalities stands due to the arbitrary selection of $x_{-k}, \ldots, x_{-1}$ ($HrS_{-k} = 0$ if $x_{-k} = x_{-k+1} = \cdots = x_{-1} = 1 - \frac{1}{A}$ and $A = 1$).

Let us assume that the rank of subsequence S_j is $HrS_j = m$; $m < +\infty$. Then it is possible to construct the characteristic determinant of the subsequence S_j [18]:

$$\Delta^{(m)} S_j(\rho) := \begin{vmatrix} x_j & x_{j+1} & \cdots & x_{j+m} \\ x_{j+1} & x_{j+2} & \cdots & x_{j+m+1} \\ & & \cdots & \\ x_{j+m-1} & x_{j+m} & \cdots & x_{j+2m-1} \\ 1 & \rho & \cdots & \rho^m \end{vmatrix} \tag{13}$$

and the characteristic algebraic equation of the subsequence S_j [18]:

$$\Delta^{(m)} S_j(\rho) = 0 \tag{14}$$

Then the following two statements can be formulated:

(i) The characteristic equation (14) has roots $\rho_k \in C$; $k = 1,2,\ldots,r$. The recurrence indexes of these roots n_k; $n_k \in N$ satisfy the equality $n_1 + n_2 + \cdots + n_r = m$.

(ii) Such coefficients $\bar{\rho}_1, \bar{\rho}_2, \ldots, \bar{\rho}_{\bar{r}}$ and μ_{kl} $(k = 1,2,\ldots,\bar{r};\ l = 1,2,\ldots,\bar{n}_{\bar{r}})$ exist with which the following equality holds true:

$$x_n = \sum_{k=1}^{\bar{r}} \sum_{l=0}^{\bar{n}_k - 1} \mu_{kl} \binom{n}{l} \rho_k^{n-l}; \quad n = j, j+1, j+2, \ldots. \tag{15}$$

Theorem 1. *Statements (i) and (ii) are equivalent; moreover* $r = \bar{r}$; $\rho_k = \bar{\rho}_k$ *and* $n_k = \bar{n}_k$.

The rigorous proof of Theorem 1 is given in [18].

Let us assume that a subsequence S_j satisfies statements (i) and (ii). Then roots $\rho_1, \rho_2, \ldots, \rho_r$ and their recurrences $n_1, n_2, \ldots, n_r$ can be solved from Eq. (14). Now, coefficients μ_{kl} can be determined from a system of linear algebraic equations which can be formed from equalities Eq. (15) assuming the expressions of elements $x_{n_1}, x_{n_2}, \ldots, x_{n_m}$ of the subsequence S_j where indexes of these elements satisfy inequalities $j \leqslant n_1 < n_2 < \cdots < n_m < +\infty$. Moreover, such system of linear algebraic equations has one and only solution.

Definition 4. The set of elements $x_j, x_{j+1}, x_{j+2}, \ldots, x_{j+m}$ which do satisfy Eq. (15) is called a fragment of algebraic progression.

Algebraic progressions generalize arithmetic progressions $(a_0 + jd; j \in Z_0)$ with $Hr(a_0 + jd; j \in Z_0) = 2$ and geometric progressions $(a_0\lambda^j; j \in Z_0)$ with $Hr(a_0\lambda^j; j \in Z_0) = 1$.

Definition 5. A subsequence S_j is an algebraic progression if its all elements satisfy equalities in Eq. (15).

Corollary 4. *A chaotic sequence does not have a rank.*

The proof is straightforward. Let us assume that a chaotic sequence has a rank. Then, according to Theorem 1, it is an algebraic progression. Thus, the dynamics of the sequence is deterministic, what contradicts the definition of a chaotic sequence.

3. Computation of ranks for the logistic map

Logistic map is a paradigmatic model used to illustrate the evolution of a simple nonlinear system to chaos [22]. This discrete dynamical map comprises one control parameter A; we will investigate the interval $0 \leqslant A \leqslant 4$:

$$x_{n+1} = F(x_n) = Ax_n(1 - x_n) \tag{16}$$

The properties of the logistic map are well and thoroughly explored. A single stable fixed point $x = 0$ exists at $0 \leqslant A \leqslant 1$. The equation

$$x = F(x) \tag{17}$$

yields two solutions at $A > 1$: $x^{(1)} = 0$ and $x^{(2)} = 1 - \frac{1}{A}$. The fixed point $x^{(1)}$ becomes unstable at $A > 1$ because the derivative $\left.\frac{dF(x)}{dx}\right|_{x=x^{(1)}}$ becomes higher than 1 (the necessary condition for a fixed point x^* to be stable reads $\left|\left.\frac{dF(x)}{dx}\right|_{x=x_*}\right| < 1$ [22]). The fixed point $x^{(2)}$ remains stable until $1 < A \leqslant 3$. The derivative $\left.\frac{dF(x)}{dx}\right|_{x=x^{(2)}}$ becomes lower than -1 at $A > 3$ and the fixed point $x^{(2)}$ becomes unstable; the first period doubling bifurcation is observed at $A = 3$. Though unstable, both fixed points $x^{(1)}$ and $x^{(2)}$ are still solutions of Eq. (17) even at $A > 3$. In other words, a period-one sequence $x^{(2)}, x^{(2)}, \ldots$ would be produced by Eq. (16) if one would start the iterative process exactly from $x_0 = x^{(2)}$ even at $3 < A \leqslant 4$.

Similar considerations can be continued for higher order period doubling bifurcations. Fixed points of the period two sequence can be found from the equality $x = F(F(x)) = F^2(x)$. The second period doubling bifurcation occurs at $A = 1 + \sqrt{6}$ when the derivative $\frac{d\left(F^2(x)\right)}{dx}$ calculated at the second fixed point of the period-two sequence becomes lower than -1. The whole cascade of period doubling bifurcations is usually visualized by plotting stable attractors at consequent discreet values of the parameter A (Fig. 1). Initially, a sufficient number of iterations are executed until transient processes cease down (for every discrete value of A) and only then the well-known stable manifold of the logistic map is visualized in Fig. 1 (a logarithmic scale for the parameter axis is used for clarity).

A sequence S_0 can be constructed as an iterative solution of the logistic map starting from the initial condition x_0 and at a fixed value of the parameter A. The algorithm used for the computation of the rank of a sequence S_0 is rather straightforward. We form a sequence of minors $H_0^{(m)}$ (Eq. (4)); $m = 2,3,\ldots$ and calculate their determinants. Theoretically, this process should be continued until such m when $\det\left(H_0^{(m)}\right) = 0$. Unfortunately, as shown in previous examples, the rank of a chaotic time series does not exist (m tends to infinity). Therefore we limit the sequence of minors setting the upper bound for m ($m = 2,3,\ldots,14$ for experiments with the logistic map). If the sequence of the determinants does not vanish until $m = 14$ we terminate the process assuming that $HrS_0 \geqslant 15$.

Though theoretically one needs to find a minor which determinant is equal to zero, in practice it suffices to compute determinants up to a certain precision, like the machine epsilon. Thus we continue the computation of determinants until $\left|\det\left(H_0^{(m)}\right)\right| < \varepsilon$ or $m > 14$. In this respect our computations reveal not the rank, but the pseudorank of a sequence (in analogy to the pseudospectrum of a linear operator [23,24]).

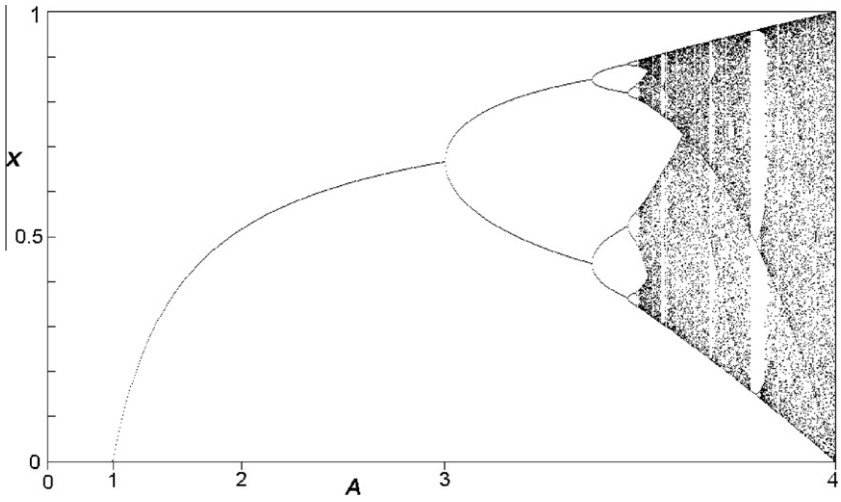

Fig. 1. The bifurcation diagram for the logistic map.

Since the iterative sequence S_0 starts from the initial condition x_0 and the logistic map comprises one control parameter A, it is possible to construct a surface of pseudoranks of solutions of the logistic map over the region $0 \leqslant x_0 \leqslant 1$; $0 \leqslant A \leqslant 4$. Such surface in color levels for $\varepsilon = 10^{-10}$ is shown in Fig. 2.

The fractal structure of the surface of pseudoranks in Fig. 2 reveals many interesting features. At $0 \leqslant A \leqslant 1$ the pseudorank is low around the stable fixed point $x_0 = 0$. The pseudorank is also low around the curve $x_0 = 1 - \frac{1}{A}$ at $1 \leqslant A \leqslant 4$ (x_0 is an asymptotically stable fixed point at $1 \leqslant A < 3$). The first period doubling bifurcation is clearly visible at $A = 3$. Higher order bifurcations are somewhat overshadowed by the fractal structure of the fractal partially due to the fact that the upper boundary of the pseudorank is set to 15. Anyway, a zone of the existence of the stable period-three solution can be clearly seen (after the cascade of period doubling bifurcations). In order to explain other specific characteristics of the surface of pseudoranks in Fig. 1 we return back to some basic properties of the logistic map.

4. Non-asymptotic convergence to the stable and the unstable manifolds

In general, the object of this paper is not to construct the stable or the unstable manifold – this information is automatically generated as a graphical representation after the H-rank method is employed to a discrete iterative map. But an important and somewhat unexpected result of this method is the identification of the set of points converging non-asymptotically to the stable (and the unstable manifolds).

So far we have been addressing forward iterations of the logistic map starting from an initial condition x_0 at a fixed value of the parameter A; $0 \leqslant x_1, x_2, \ldots \leqslant \frac{A}{4}$ when $0 \leqslant A \leqslant 4$. It is also possible to construct backward iterations starting from point x_{n+1}:

$$x_n^{(1,2)} = F^{-1}(x_{n+1}) = \frac{1}{2}\left(1 \pm \sqrt{1 - \frac{4x_{n+1}}{A}}\right) \tag{18}$$

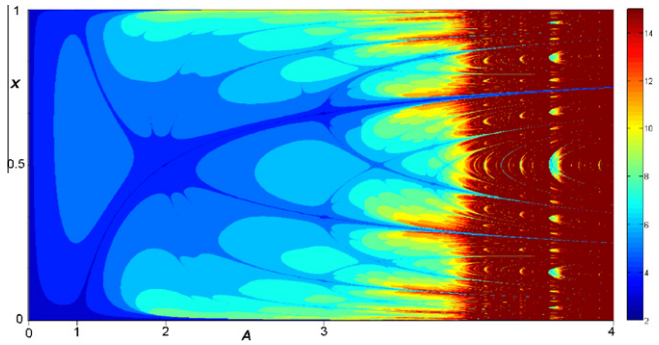

Fig. 2. The surface of pseudoranks for the logistic map; $\varepsilon = 10^{-10}$; $m = 14$.

The superscript (1,2) on the left side of Eq. (18) denotes that one point x_{n+1} may generate up to two origins $\frac{1}{2} \leqslant x_n^{(1)} \leqslant 1$ and $0 \leqslant x_n^{(2)} \leqslant \frac{1}{2}$. We will consider a backward iteration process starting from x_0 and will require that x_0 is on the stable manifold. In other words, we will seek a process which non-asymptotically converges to x_0 in a finite number of forward steps.

We will analyze the interval $1 < A \leqslant 3$ first since the stable manifold is a period-one solution described by equality $x = 1 - \frac{1}{A}$ there. Assignments $n = -1$ and $x_0 = 1 - \frac{1}{A}$ in Eq. (18) yield:

$$x_{-1}^{(1,2)} = \frac{1}{2}\left(1 \pm \left|1 - \frac{2}{A}\right|\right) \tag{19}$$

If $1 < A < 2,\ x_{-1}^{(1)} = \frac{1}{A}$ and $x_{-1}^{(2)} = 1 - \frac{1}{A} = x_0$. The process can be continued from $x_{-1}^{(1)}$:

$$x_{-2}^{(1,2)} = F^{-1}\left(x_{-1}^{(1)}\right) = \frac{1}{2}\left(1 \pm \sqrt{1 - \frac{4}{A^2}}\right) \tag{20}$$

Unfortunately, neither $x_{-2}^{(1)}$ nor $x_{-2}^{(2)}$ does not exist because $1 - \frac{4}{A^2} < 0$ when $1 < A < 2$; a backward iteration can not be executed from $x_{-1}^{(1)}$. We denote such points which can not be iterated backward as terminal points and mark them by black circles in Fig. 3. Of course, the process can be continued from $x_{-1}^{(2)}$, but the picture would be exactly the same. Thus we limit the demonstration of backward iterations by one backward step in Fig. 3.

Let us denote the manifold of non-asymptotic convergence (NAC) as a set of points from which the stable or the unstable manifold can be reached in a finite number of forward iteration steps. The unstable manifold comprises only one single terminal point $x = \frac{1}{A}$ at $1 < A < 2$.

Of course, the point $x = 1 - \frac{1}{A}$ is an asymptotically stable fixed point at $1 < A < 2$. All initial conditions from the interval $[0; 1]$ will eventually lead to the fixed point in the process of forward iterations at $1 < A < 2$. But there exists only one point (except the fixed point itself) which will lead to the fixed point in a finite number of forward iterations (this number is one).

Next we continue with $A = 2$. A single backward iteration yields $x_{-1}^{(1)} = x_{-1}^{(2)} = x_0 = \frac{1}{2}$. The forward iteration process started from any other initial point than the stable fixed point itself would require an infinite number of forward iteration steps to reach the fixed point. The NAC manifold becomes an empty set at $A = 2$.

The interval $2 < A < 3$ is analyzed next. Eq. (19) yields: $x_{-1}^{(1)} = 1 - \frac{1}{A} = x_0;\ x_{-1}^{(2)} = \frac{1}{A}$. The process can be continued from $x_{-1}^{(2)}$:

$$x_{-2}^{(1,2)} = F^{-1}\left(x_{-1}^{(2)}\right) = \frac{1}{2}\left(1 \pm \sqrt{1 - \frac{4}{A^2}}\right) \tag{21}$$

Both points $x_{-2}^{(1)}$ nor $x_{-2}^{(2)}$ exist; $0 < x_{-2}^{(2)} < x_{-2}^{(1)} < 1$ at $2 < A < 3$. It can be noted that $x_{-2}^{(1)}$ is a terminal point (Fig. 4). But the process can be continued from $x_{-2}^{(2)}$. Every successive backward iteration produces 2 points; $0 < x_{-k}^{(2)} < x_{-k}^{(1)} < 1;\ k = 2, 3, \ldots$; all $x_{-k}^{(1)}$ are terminal points; $x_{-k}^{(2)}$ are non-terminal points. Moreover, $\lim_{k\to\infty} x_{-k}^{(1)} = 1;\ \lim_{k\to\infty} x_{-k}^{(2)} = 0$ (Fig. 4).

As noted previously, the point $x = 1 - \frac{1}{A}$ becomes unstable when A exceeds 3. The first period doubling bifurcation occurs at $A = 3$. Nevertheless, the point $x = 1 - \frac{1}{A}$ is still a solution of Eq. (17) at $3 \leqslant A \leqslant 4$. An iterative process started exactly at $x_0 = 1 - \frac{1}{A}$ will generate a period-one sequence in the whole interval $2 \leqslant A \leqslant 4$. Therefore, similar backward iterations analysis can be performed in the interval $3 \leqslant A \leqslant 4$ since we build a NAC manifold for the period-one forward sequence (we do not investigate asymptotic stability of this period-one forward sequence).

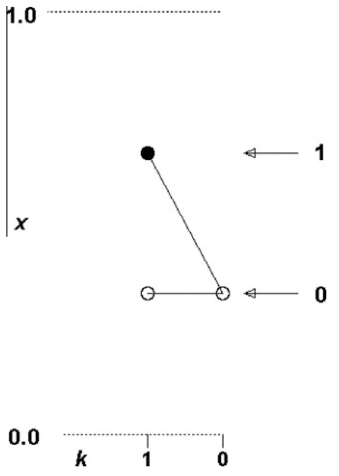

Fig. 3. A backward iteration from a period-one fixed point $x_0 = 1 - \frac{1}{A}$ at $A = 1.5$; k denotes the backward number; x-axis is on the left. Arrows at right point at two origins; numbers at arrows denote the number of forward iterations needed to reach x_0 from appropriate origin; the black circle denotes the terminal point.

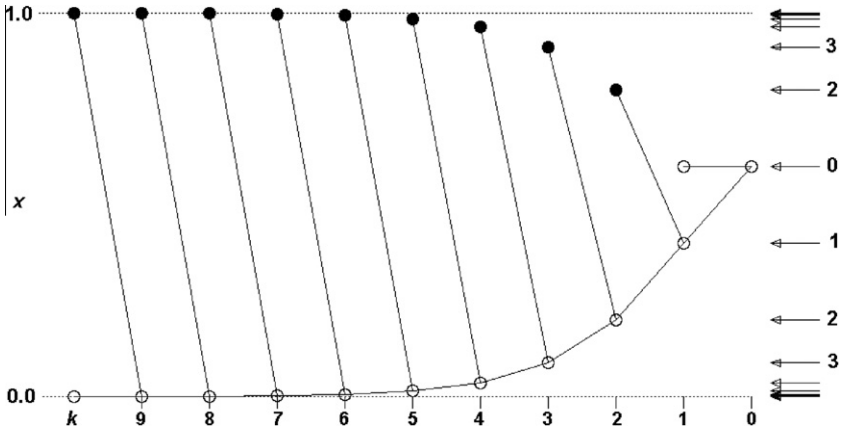

Fig. 4. The unstable manifold for the period-one fixed point at $A = 2.5$.

The period-one stable manifold (a dashed line) and the NAC manifold (solid lines) are illustrated in Fig. 5. The stable and the NAC manifolds intersect at point $A = 2$. A bifurcation of the NAC manifold occurs and gives birth to an infinite number of points in the backward iteration process. In other words, an infinite number of initial conditions would lead to period-one process at $A > 2$. It must be noted that asymptotic convergence to the stable period-one process is not considered here. We consider non-attracting evolutions instead:

$$x_{-k}, x_{-k+1}, x_{-k+2}, \ldots, x_{-2}, x_{-1}, \left(1 - \frac{1}{A}\right), \left(1 - \frac{1}{A}\right), \ldots \tag{22}$$

Index k in Eq. (22) determines how much forward iterations are needed to reach the period-one process. Solid 5 pixels thickness lines stand for initial conditions which lead to the period-one process in one forward step; 4 pixels thickness lines stand for initial conditions which lead to the period-one process in two forward steps; 3 pixels thickness lines – in three forward steps; 2 pixels thickness lines – in 4 forward steps; and finally 1 pixel thickness line – in 5 forward steps. In general, the infinite uncountable set of initial conditions in the interval $[0;1]$ can be classified to an infinite countable set of initial conditions which lead (not asymptotically) to the period-one process in a finite number of forward iterations at $2 < A \leqslant 4$ and an infinite uncountable set of initial conditions which asymptotically lead to the period-one process in an infinite number of forward iterations (at $2 < A < 3$) or lead to other evolutions (at $3 < A \leqslant 4$).

Clearly, the pseudorank is low also along the curve $x_0 = \frac{1}{A}$ (at $1 \leqslant A \leqslant 4$). It denotes all initial conditions leading (non-asymptotically) to the period-one solution in one forward iteration. Moreover, one can clearly observe the bifurcation of the unstable manifold at $A = 2$ which generates an infinite number of initial conditions leading (non-asymptotically) to the period-one solution in a finite number of steps (compare to Fig. 2).

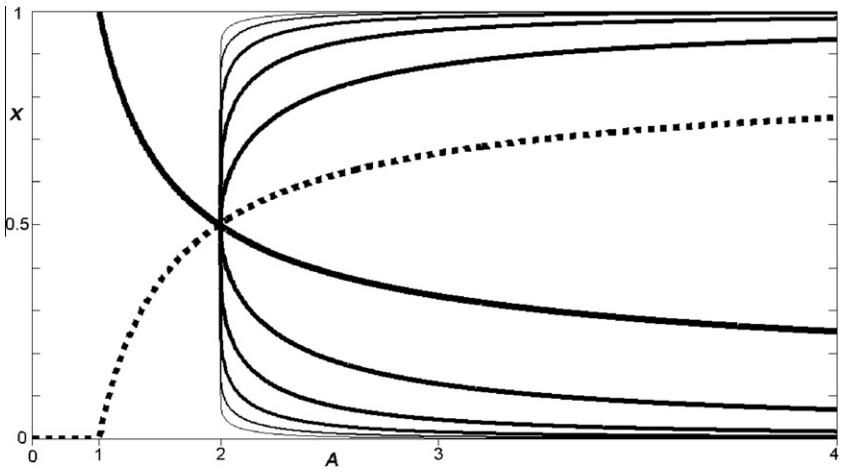

Fig. 5. The period-one solution (the dotted line) and the unstable manifold of the period-one solution for the logistic map: 5 pixels thickness solid line denotes initial conditions leading to the period-one solution in one forward iteration; 4 pixels line – in 2 forward iterations; 3 pixels line – in 3 iterations; 2 pixels line – in 4 iterations and 1 pixel line – in 5 iterations.

Analogously, it is possible to follow the evolution of a NAC manifold for the period-two solution. We omit details for the brevity, but the NAC manifold of the period-two solution can be clearly observed in Fig. 2. The infinite uncountable set of initial conditions in the interval [0;1] can be classified to an infinite countable set of initial conditions which lead (not asymptotically) to the period-two process in a finite number of forward iterations at $3 < A \leqslant 4$ and an infinite uncountable set of initial conditions which asymptotically lead to the period-two process in an infinite number of forward iterations (at $3 < A < 1 + \sqrt{6}$) or lead to other evolutions (at $1 + \sqrt{6} < A \leqslant 4$). Actually, ghosts of the first pitchfork bifurcation can be clearly seen in Fig. 2 at $3 < A < 1 + \sqrt{6}$. The process can be continued for higher order bifurcations. Nevertheless it is important to note that the period-two solution, though unstable, is still a solution of the logistic map even at $1 + \sqrt{6} < A \leqslant 4$. The traces of initial conditions leading (non-asymptotically) to the period-two solution in a finite number of steps can be clearly seen in Fig. 2.

This fact is illustrated in Fig. 6 where the schematic diagram of the stable, the unstable and the NAC manifolds are illustrated around the first period doubling bifurcation of the logistic map (the background grayscale image is copied from Fig. 2). Thick solid lines denoted by the symbol *S* represent the stable manifold. The thick dotted line denoted by the symbol *U* represents the unstable manifold. Thick widely dashed lines denoted by symbols *NAC-S* represent the part of the NAC manifold which converges non-asymptotically to the stable manifold. In fact we did illustrate only the top and the bottom traces of the pitchfork bifurcation in Fig. 6 (though repetitive higher order traces are clearly visible also).

Thick narrowly dashed lines denoted by symbols *NAC-U* represent the part of the NAC manifold which converges non-asymptotically to the unstable manifold. Such non-asymptotic convergence to the unstable manifold can be illustrated by a simple example. It is clear that a point $x_0 = \frac{3}{4}$ belongs to the unstable manifold at $A = 4$ (it is period-1 unstable fixed point; the forward iterative process started at this point continues infinitely). Then, the point $x_{-1}^{(2)} = \frac{1}{4}$ belongs to the part of the NAC manifold which converges non-asymptotically to $\frac{3}{4}$. Really, forward iterations started from $\frac{1}{4}$ (at $A = 4$) yield a sequence $\frac{1}{4}, \frac{3}{4}, \frac{3}{4}, \ldots$.

Another interesting observation can be done regarding the intersection of the bottom branch of the stable manifold and the upper branch of *NAC-S* in Fig. 6. The intersection between the stable and the NAC manifolds results into the bifurcation of the NAC manifold (compare to Fig. 5). In other words, the surface of pseudoranks reveals the fractal structure of three intertwined manifolds: the stable, the unstable and the NAC manifolds. Such representation, though easy to compute, reveals rich and complex dynamical structure of the logistic iterated map.

In other words, the surface of pseudoranks reveals the structure of the stable, the unstable and the NAC manifolds intertwined. Such representation, though easy to compute, reveals rich dynamical structure of the iterated map.

5. The selection of the upper bound of the rank for a discrete iterated map

So far we had selected the upper bound of the rank for the logistic map $m = 14$ (we terminate the computation of the sequence $\det(H_0^{(m)})$; $m = 2, 3, \ldots$ if determinants do not vanish until $m = 14$). The selection of this concrete upper bound requires additional explanations.

First of all we repeat the computational experiment and construct the surface of pseudoranks for the logistic map setting $m = 5$ (it is assumed that $HrS_0 \geqslant 6$ if the sequence of determinants does not vanish until $m = 5$). Such a surface in color levels for $\varepsilon = 10^{-10}$ is shown in Fig. 7. Next, we repeat the procedure setting $m = 20$ (Fig. 8).

Figs. 2, 7 and 8 clearly reveal the role of the parameter m. The upper bound of the rank for a discrete iterative map plays the role of a focus in a virtual optical system. The value of the parameter m determines the region where the attention is concentrated (under the constraints of the visualization scheme employing a finite number of color levels). The first period-doubling bifurcation is well visualized in Fig. 7. But it is almost impossible to distinguish the second period-doubling

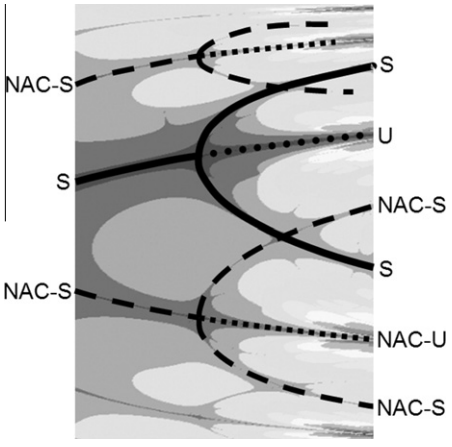

Fig. 6. A schematic diagram illustrating the stable, the unstable and the NAC manifolds in the region around the first period doubling bifurcation of the logistic map.

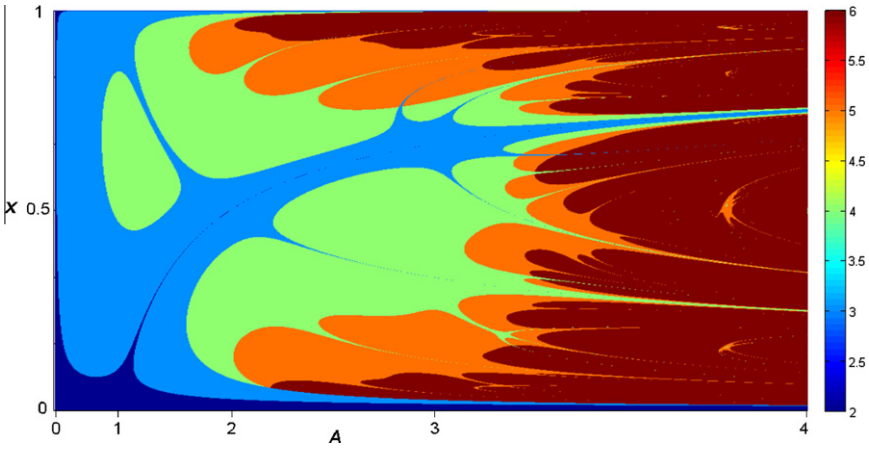

Fig. 7. The surface of pseudoranks for the logistic map: $\varepsilon = 10^{-10}$; $m = 5$.

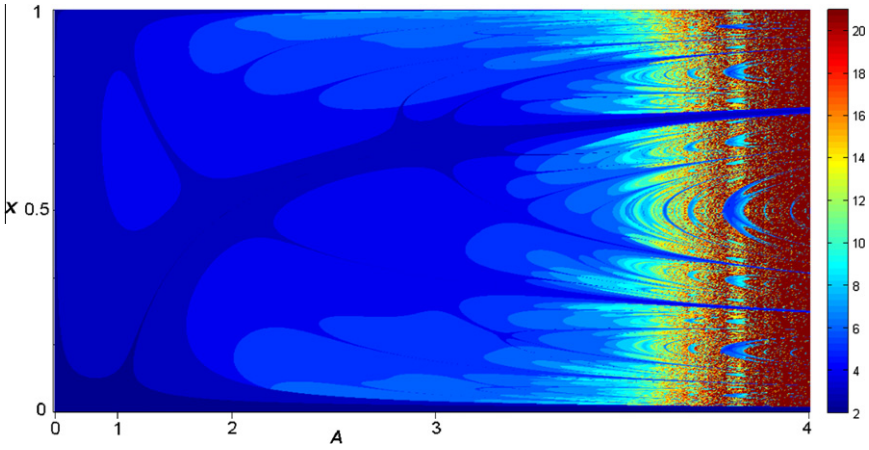

Fig. 8. The surface of pseudoranks for the logistic map: $\varepsilon = 10^{-10}$; $m = 20$.

bifurcation (and higher bifurcations) simply because the complexity of these transient processes is higher than the preselected value of $m = 5$.

It is hard to distinguish the cascade of period doubling bifurcations and the onset to chaos in Fig. 8 also. The preselected value $m = 20$ helps to visualize the sensitivity to initial conditions in the chaotic region, but the transition to chaos is compressed into a small interval of discrete color levels. The transition to chaos is much better visualized at $m = 14$ (Fig. 2).

It can be noted that the upper bound of the rank for a discrete iterated map must be preselected individually for each different discrete iterative map. Several experiments with different values of m are required before one can select the optimal resolution of a region of interest.

6. The rank of a solution as an indicator of chaos

The pseaudorank can be calculated also for a subsequence of the solution S_j; $j > 0$ (Eq. (2)). We repeat the computational experiment illustrated in Fig. 2, but now we wait until the transient processes cease down before commencing the computation of the rank of the subsequence (we use $j = 1000$). The sequence of minors now is $H_j^{(m)}$ (Eq. (4)); $m = 2, 3, \ldots$; the upper bound of the rank is again 15.

The resulting pseudorank distribution is shown in Fig. 9. Naturally, all information about transient processes is lost.

The lowest rank corresponds to the period-one solution in the interval $0 < A < 3$ (Fig. 9). Period-two and period-four solutions are also well-expressed in Fig. 9. But the rank becomes sensitive to the initial condition (though even a long initial sequence is omitted) after the cascade of period doubling bifurcations. Such sensitivity of the rank to initial conditions can not be explained only by the fact that the duration of transient processes tends to infinity for a chaotic solution of a deterministic dynamical system. This is also due to the fact that stable and unstable manifolds for different period length solutions get intertwined after the cascade of period doubling bifurcations. Such topological phenomenon can be exploited for the

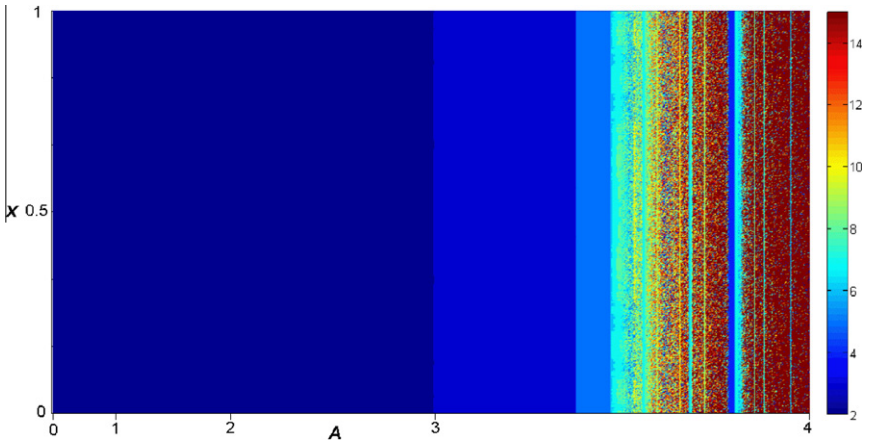

Fig. 9. The surface of pseudoranks of subsequences for the logistic map; $j = 1000$; $\varepsilon = 10^{-10}$; $m = 14$.

construction of a new detector of chaos in a discrete nonlinear dynamical system. One should fix system's parameters, change initial conditions, compute pseudoranks of subsequencies omitting transient processes and, finally, determine the standard deviation of the computed pseudoranks. The equality of the standard deviation to zero marks the insensitivity to initial conditions. Remarkably, such a detector does not discriminate asymptotic or non-asymptotic convergence (if transient processes are omitted of course). But the occurrence of chaotic processes is immediately detected as the standard deviation gets positive (Fig. 10). The magnitude of the standard deviation denotes the topological sensitivity to initial conditions and represents the essence of the definition of deterministic chaos. By the way, one should not be confused by the negative slope of the standard deviation when A approaches 4 in Fig. 10. We have computed pseudoranks using the upper limit. The standard deviation will be low if the rank is higher than the preset limit in the majority of points.

Natural is the question why a new computational detector of deterministic chaos in a discrete nonlinear system should be coined if classical and well-validated computational tools already exist for that purpose. Calculation of the Lyapunov exponent for the logistic map is a benchmark exercise for anyone who gets acquainted with nonlinear dynamics in general. The Lyapunov exponent λ for an orbit of the logistic map starting at x_0 reads [25]:

$$\lambda(A, x_0) = \lim_{n\to\infty} \frac{1}{n} \sum_{k=0}^{n-1} \log |A(1 - 2x_k)| \tag{23}$$

In practice, one should start the forward iteration process from x_0, continue for a sufficient number of time steps, and then compute λ for a sufficiently large number of iterates of the subsequence. But what would happen if $A = 4$ and $x_0 = \frac{3}{4}$?

The Lyapunov exponent of an orbit starting at x_0 in dependence of A produces a general view of the system's sensitivity to initial conditions. In fact, a sweep over the range of values of the parameter A (at fixed x_0) cuts through a web of orbits which converge non-asymptotically (in a finite number of steps) to orbits of finite period lengths. More accurate results would be

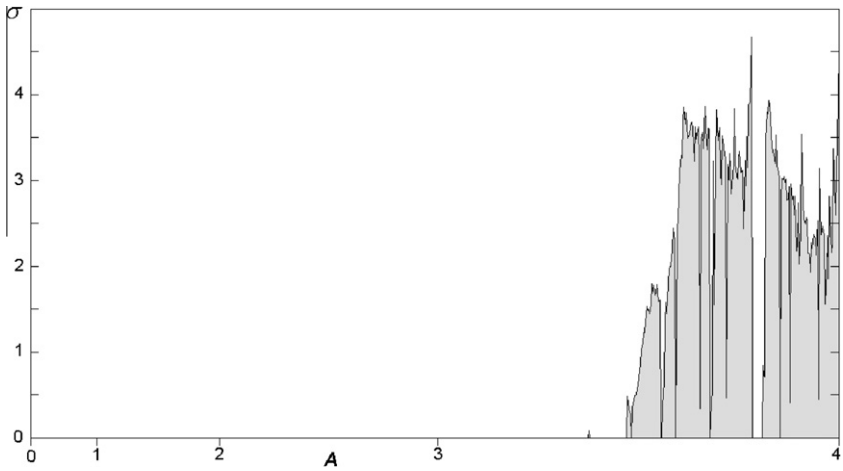

Fig. 10. The standard deviation of the rank of subsequences for the logistic map detects the sensitivity to initial conditions.

produced if the Lyapunov exponent would be calculated from many different starting points and then averaged for every value of the parameter A. But then the process would become computationally costly.

Our method, on the contrary to the Lyapunov exponent, does not show if an attractive periodic orbit exists. As mentioned previously, it exhibits only the system's sensitivity to initial conditions. In addition, this method can reveal the pattern of stable and unstable manifolds intertwined, what can be a qualitative advantage in certain cases.

7. Computation of ranks for the Henon map

So far the logistic map has been analyzed. We will test the functionality of the proposed indicator of chaos based on the rank of solutions using another paradigmatic system – the discrete Henon map described by two iterative equations [26,27]:

$$\begin{aligned} x_{n+1} &= y_n + 1 - ax_n^2 \\ y_{n+1} &= bx_n \end{aligned} \tag{24}$$

The Henon map depends on two parameters a and b and maps a point (x_n, y_n) in the plane to a new point iteratively. Parameters for the canonical Henon map have values of $a = 1.4$ and $b = 0.3$; for the canonical values the Henon map is chaotic. As a dynamical system, the Henon map is interesting because, unlike the logistic map, its orbits defy a simple description.

First of all we construct the orbit diagram for the Henon map with $b = 0.3$ and $1 \leqslant a \leqslant 1.4$; values of y in every second forward iteration (after transient had ceased down) are shown in Fig. 11. Next we plot the surface of ranks calculated with $b = 0.3$; $1 \leqslant a \leqslant 1.4$; $x_0 = 0$ and $-0.2 \leqslant y_0 \leqslant 0.2$; the upper bound of the rank is set to 24; interesting intertwined patterns can be observed in Fig. 12. Plotting the surface of pseudoranks of subsequences ($j = 1000$) reveals the systems's sensitivity to initial conditions (Fig. 13). Finally, the standard deviation of the rank of subsequences for the Henon map helps to identify the onset to chaos (Fig. 14).

A zoo of different discrete iterative maps could be analyzed by the H-rank method, but we would like to concentrate the attention of the reader to another question. Whenever a new method is proposed for whatever purpose, a natural question arises – what new information this method can reveal and why should it be used instead of other existing methods. At this point we would like to refer to a recent paper by Bresten and Jae-Hun [4] where the physical measurement of the speed of convergence is exploited to build the non-asymptotic convergence manifold of the logistic map in the most trivial range of the control parameter of the logistic map. The construction of the manifold of non-asymptotic convergence in the region of period-doubling bifurcations, the regions around the Feigenbaum attractor and beyond is left as an object of further research in [4]. The H-rank method is a perfect solution for these purposes; it does not differentiate if the system is in the period-1 region, the region around the Feibenbaum attractor or at $A = 4$. The universality, simplicity and straightforwardness of the H-rank method opens new possibilities for the investigation of properties of convergence of discrete iterative maps.

8. Concluding Remarks

The rank of a sequence appears to be an effective computational tool for the investigation of discrete nonlinear dynamical systems. It reveals the embedded complexity of the algebraic progression in the analyzed sequence. The computation and visualization of pesudoranks in the space of system's parameters and initial conditions reveals three manifolds of a discrete iterative map: the stable manifold, the unstable manifold and the manifold of the non-asymptotic convergence. All these manifolds are produced by a simple and a straightforward computational rule. The essential property of this method is that

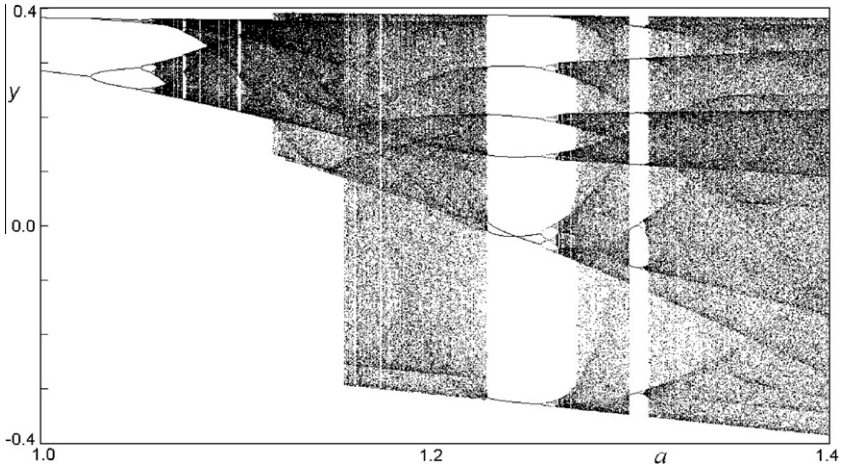

Fig. 11. Orbit diagram for the Henon map with $b = 0.3$ and $1 \leqslant a \leqslant 1.4$.

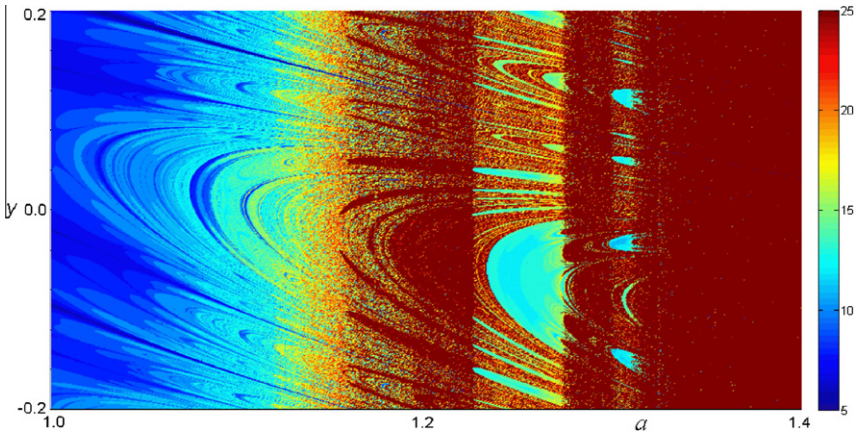

Fig. 12. The surface of pseudoranks for the Henon map; $\varepsilon = 10^{-10}$; $m = 24$.

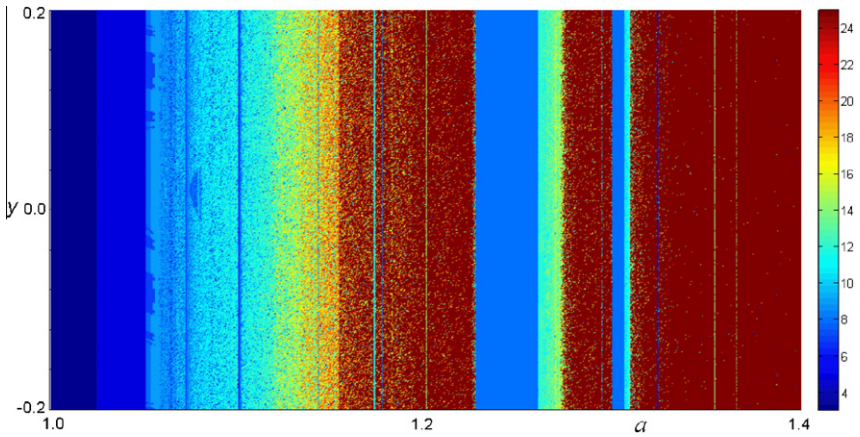

Fig. 13. The surface of pseudoranks of subsequences for the Henon map; $j = 1000$; $\varepsilon = 10^{-10}$; $m = 24$.

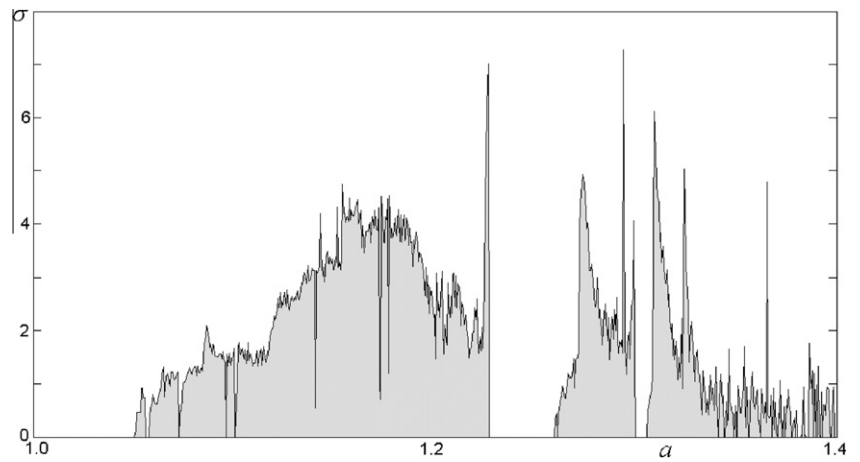

Fig. 14. The standard deviation of the rank of subsequences for the Henon map detects the sensitivity to initial conditions.

all three manifolds are produced simultaneously and are of course intertwined in one figure. One does not have to employ a reverse iteration process or to physically count the speed of convergence in order to construct the NAC manifold. No special techniques are required for the visualization of the unstable manifold either. Thus the H-rank method outperforms existing methods proposed for clocking the convergence of discrete maps and provides a deeper insight into dynamical processes taking place in discrete iterative maps. The H-rank method is completely a numerical technique. Thus the selection of the upper bound of the rank, the selection of the machine epsilon, the selection of the appropriate window of system's parameters and initial conditions is left for the responsibility of the user and must be adapted for every single discrete iterative map. Nonetheless, the H-rank method provides a simple and effective numerical tool for qualitative investigation of discrete iterative maps.

References

[1] de Moura FABF, Tirnakli U, Lyra ML. Convergence to the critical attractor of dissipative maps: long-periodic oscillations, fractality, and nonextensivity. Phys Rev E 2000;62:6361–5.
[2] Tonelli R, Coraddu M. Numerical study of the oscillatory convergence to the attractor at the edge of chaos. Eur Phys J B 2006;50:355–9.
[3] Robledo A, Moyano LG. *q*-Deformed statistical-mechanical property in the dynamics of trajectories en route to the Feigenbaum attractor. Phys Rev E 2008;77:036213.
[4] Bresten CL, Jae-Hun Jung. A study on the numerical convergence of the discrete logistic map. Commun Nonlinear Sci Numer Simul 2009;14:3076–88.
[5] Ho BL, Kalman RE. Effective construction of linear state-variable models from input–output functions. Regelungstechnik 1965;12:545–8.
[6] de Jong LS. Numerical aspects of recursive realization algorithms. SIAM J Contr Optim 1978;16:646–59.
[7] Akaike H. Stochastic theory of minimal realization. IEEE Trans Automat Contr 1974;26:667–73.
[8] Gevers M, Kailath T. An innovations approach to least-squares estimation, Part vi: Discrete-time innovations representations and recursive estimation. IEEE Trans Automat Contr 1973;18:588–600.
[9] Juang J, Pappa R. An eigensystem realization algorithm for modal parameter identification and model reduction. J Guid Contr Dyn 1985;8:620–7.
[10] Gohberg I, Kaashoek MA, Lerer L. On minimality in the partial realization problem. Syst Contr Lett 1987;9:97–104.
[11] Hinrichsen D, Manthey W, Helmke U. Minimal partial realization by descriptor systems. Linear Algebra Appl 2001;326:45–84.
[12] Bakule L, Rodellar J, Rossell JM. Controllability—observability of expanded composite systems. Linear Algebra Appl 2001;332:381–400.
[13] Chaib S, Boutat D, Benali A, Barbot JP. Observability of the discrete state for dynamical piecewise hybrid systems. Nonlinear Anal: Theor Methods Appl 2005;63:423–38.
[14] Coll C, Fullana MJ, Sanchez E. Reachability and observability indices of a discrete-time periodic descriptor system. Appl Math Comput 2004;153:485–96.
[15] De la Sen M. On minimal realizations and minimal partial realizations of linear time-invariant systems subject to point incommensurate delays. Math Prob Eng 2008;2008. Article ID 790530, 19 p..
[16] Carniel R, Barazza F, Tarraga M, Ortiz R. On the singular values decoupling in the singular spectrum analysis of volcanic tremor at Stromboli. Nat Hazards Earth Syst Sci 2006;6:903–9.
[17] Layman JW. The Hankel transform and some of its properties. J Integer Seq 2001;4. Article 01.1.5..
[18] Navickas Z, Bikulciene L. Expressions of solutions of ordinary differential equations by standard functions. Math Model Anal 2006;11:399–412.
[19] Navickas Z, Ragulskis M. How far one can go with the Exp-function method? Appl Math Comput 2009;211:522–30.
[20] Navickas Z, Bikulciene L, Ragulskis M. Generalization of Exp-function and other standard function methods. Appl Math Comput 2010;216:2380–93.
[21] Navickas Z, Ragulskis M, Bikulciene L. Be careful with the Exp-function method – Additional remarks. Commun Nonlinear Sci Numer Simul 2010;15:3874–86.
[22] Weisstein EW. Logistic Map. From MathWorld-A Wolfram Web Resource. Available at: <http://mathworld.wolfram.com/LogisticMap.html>.
[23] Trefethen LN. Computation of pseudospectra. Acta Numer 1999;8:247–95.
[24] Trefethen LN. Pseudospectra of linear operators. SIAM Rev 1997;39:383–406.
[25] Hilborn RC. Chaos and nonlinear dynamics – an introduction for scientists and engineers. Norfolk: Oxford University Press; 2004.
[26] Henon M. A two-dimensional mapping with a strange attractor. Commun Math Phys 1976;50:69–77.
[27] Cvitanovic P, Gunaratne G, Procaccia I. Topological and metric properties of Henon-type strange attractors. Phys Rev A 1988;38:1503–20.